Joint short- and long-baseline constraints on light sterile neutrinos

F. Capozzi,[1,2] C. Giunti,[3] M. Laveder,[1,2] and A. Palazzo[4,5]

[1]*Dipartimento di Fisica e Astronomia "Galileo Galilei," Università di Padova,*
Via F. Marzolo 8, I-35131 Padova, Italy
[2]*Istituto Nazionale di Fisica Nucleare (INFN), Sezione di Padova, Via F. Marzolo 8, I-35131 Padova, Italy*
[3]*Istituto Nazionale di Fisica Nucleare (INFN), Sezione di Torino, Via P. Giuria 1, I-10125 Torino, Italy*
[4]*Dipartimento Interateneo di Fisica "Michelangelo Merlin," Via Amendola 173, 70126 Bari, Italy*
[5]*Istituto Nazionale di Fisica Nucleare, Sezione di Bari, Via Orabona 4, 70126 Bari, Italy*
(Received 4 January 2017; published 17 February 2017)

Recent studies provide evidence that long-baseline (LBL) experiments are sensitive to the extra CP phases involved with light sterile neutrinos, whose existence is suggested by several anomalous short-baseline (SBL) results. We show that, within the $3+1$ scheme, the combination of the existing SBL data with the LBL results coming from the two currently running experiments, NOνA and T2K, enables us to simultaneously constrain two active-sterile mixing angles, θ_{14} and θ_{24}, and two CP phases, $\delta_{13} \equiv \delta$ and δ_{14}, although the information on the second CP phase is still weak. The two mixing angles are basically determined by the SBL data, while the two CP phases are constrained by the LBL experiments, once the information coming from the SBL setups is taken into account. We also assess the robustness or fragility of the estimates of the standard 3-flavor parameters in the more general $3+1$ scheme. To this regard we find that (i) the indication of CP violation found in the 3-flavor analyses persists also in the $3+1$ scheme, with $\delta_{13} \equiv \delta$ having still its best-fit value around $-\pi/2$, (ii) the 3-flavor weak hint in favor of the normal hierarchy becomes even less significant when sterile neutrinos come into play, (iii) the weak indication of nonmaximal θ_{23} (driven by NOνA disappearance data) persists in the $3+1$ scheme, where maximal mixing is disfavored at almost the 90% C.L. in both normal and inverted mass hierarchy, and (iv) the preference in favor of one of the two octants of θ_{23} found in the 3-flavor framework (higher octant for inverted mass hierarchy) is completely washed out in the $3+1$ scheme.

I. INTRODUCTION

The massive nature of neutrinos and their mixing has been established by a plethora of experiments performed in the last two decades with natural and artificial neutrino sources. The 3-flavor paradigm has been gradually recognized as the sole framework able to account for all the observations performed at baselines longer than ~100 meters. In contrast, the same scheme is not able to explain a series of results recorded at shorter distances dubbed as short-baseline (SBL) anomalies. One possible explanation of the SBL anomalies is provided by a flavor oscillation process mediated by new hypothetical light sterile neutrino states, albeit this hypothesis encounters some difficulties in explaining simultaneously all the existing data sets. In particular, a non-negligible statistical tension emerges when one compares the (positive) $\nu_\mu \to \nu_e$ appearance signals with the joint disappearance results from the (positive) searches in the $\nu_e \to \nu_e$ channel and the (negative) ones in the $\nu_\mu \to \nu_\mu$ channel.

In the so-called $3+1$ scheme, only one new (essentially sterile) mass eigenstate is introduced, with a squared-mass splitting of the order of $\Delta m_{\mathrm{SBL}}^2 \sim 1$ eV^2 with respect to the three standard neutrinos. In such a scheme the active-sterile admixture is supposed to be small but large enough to explain the anomalies. The $3+1$ scheme predicts, by construction, sizable effects at the short distances, where the oscillating factor $\Delta_{\mathrm{SBL}} = \Delta m_{\mathrm{SBL}}^2 L/4E$ (L being the baseline and E the neutrino energy) is of order one. A rich program of new SBL experiments is underway with the purpose of detecting the smoking gun of active-sterile neutrino oscillations, i.e., the characteristic L/E dependence of the events rate.

After a hypothetical discovery of a sterile neutrino at SBL experiments, the full exploration of the properties of these particles would need other types of experimental setups. In particular, the SBL experiments would not be able to provide any information on the CP phases involved in the $3+1$ scheme. In fact, the manifestation of CP-violation (CPV) is intimately related to the interference of two distinct frequencies. At the SBL setups only one frequency is observable (the new one), while the other two (atmospheric and solar) are undetectable. Therefore, the SBL searches are blind to the CP phases involved in the $3+1$ scheme.[1]

---

[1]In the $3 + N_s$ schemes with $N_s > 1$, CPV could be observed at SBL experiments. However, these setups can probe only a limited number of all the CP phases involved in the model. In contrast, LBL experiments have access to all such phases. For example, in the $3+2$ scheme, the SBL experiments are sensitive only to one CP phase over a total of five CP phases.

In the standard 3-flavor framework the CPV is encoded by the *CP*-phase δ which enters the leptonic mixing matrix. The 3-flavor CPV searches are performed at the long-baseline (LBL) experiments, which can observe the $\nu_\mu \to \nu_e$ transition probability in both the neutrino and antineutrino channels. These setups are designed to maximize the amplitude of the interference between the solar and atmospheric oscillations, which embodies a dependency on the *CP*-phase δ. As a matter of fact, we have already some intriguing indications on δ coming from the partial [1,2] (including only LBL data) and global [3–6] analyses, which all point towards nearly maximal CPV with $\delta \sim -\pi/2$. This trend has been recently corroborated by the latest data released by NOνA [7] and T2K [8] at the Neutrino and ICHEP 2016 conferences.

As first evidenced in Ref. [1], in the presence of light sterile neutrinos, the $\nu_\mu \to \nu_e$ transition probability probed at the LBL facilities acquires a new interference term, arising from the interference between the atmospheric frequency and the new large frequency related to the sterile state. Although the fast oscillations driven by the new frequency are completely averaged out by the finite energy resolution of the detector, nonetheless, they can leave their footprints in the transition probability. This renders the LBL experiments sensitive also to the extra *CP* phases involved in the 3 + 1 scheme. The recent 4-flavor analyses [1,2] of the data from NOνA and T2K have clearly shown that these two experiments are already sensitive to one of the new *CP* phases provided that the active-sterile mixing angles are fixed at their best-fit values determined by the SBL 3 + 1 fits [9–12]. In addition, the prospective study performed in [13] has shown that the sensitivity to the extra *CP* phases is expected to improve when NOνA and T2K will reach their full exposures, and will further increase in the next-generation experiment DUNE [14].

In this work, we stick to the real data and take a step forward with respect to the existing works. Instead of fixing the active-sterile mixing angles at their best-fit values, we here incorporate a full analysis of all the existing SBL data in combination with the LBL results. In this way, we are able to simultaneously constrain the two active-sterile mixing angles θ_{14} and θ_{24} and the two *CP* phases $\delta_{13} \equiv \delta$ and δ_{14}. The estimates of the two new mixing angles will be basically determined by the SBL data, while those of the two *CP* phases will derive from the LBL experiments, once the information from the SBL setups is considered. In this work, we also assess the robustness or fragility of the estimates of the standard 3-flavor parameters in the more general 3 + 1 scheme, paying particular attention to the most important properties currently under scrutiny: the mass hierarchy, the *CP* phase δ, and the atmospheric mixing angle θ_{23}.

The rest of the paper is organized as follows. In Sec. II, we briefly introduce the theoretical 3 + 1 framework. In Sec. III, we recall the basic features of the flavor oscillations at short baselines. Section IV deals with the 4-flavor transition probability relevant for the LBL setups. In Sec. V, we list the data used in the simulations and describe the details of their numerical analysis. In Sec. VI, we present and discuss the results of the analysis. Finally, in Sec. VII, we draw our conclusions.

II. THEORETICAL FRAMEWORK

In the 3 + 1 scheme, the flavor (ν_e, ν_μ, ν_τ, ν_s) and mass eigenstates (ν_1, ν_2, ν_3, ν_4) are related through a 4×4 mixing matrix, which we parametrize as

$$U = \tilde{R}_{34}R_{24}\tilde{R}_{14}R_{23}\tilde{R}_{13}R_{12}, \qquad (1)$$

where R_{ij} ($\tilde{R}_{ij}$) is a real (complex) 4×4 rotation in the (i, j) plane, which contains the 2×2 matrix

$$R_{ij}^{2\times2} = \begin{pmatrix} c_{ij} & s_{ij} \\ -s_{ij} & c_{ij} \end{pmatrix} \qquad \tilde{R}_{ij}^{2\times2} = \begin{pmatrix} c_{ij} & \tilde{s}_{ij} \\ -\tilde{s}_{ij}^* & c_{ij} \end{pmatrix}, \qquad (2)$$

in the (i, j) sub-block, where we have introduced the definitions

$$c_{ij} \equiv \cos\theta_{ij} \quad s_{ij} \equiv \sin\theta_{ij} \quad \tilde{s}_{ij} \equiv s_{ij}e^{-i\delta_{ij}}. \qquad (3)$$

The parameterization in Eq. (1) has the following features: i) When all the three mixing angles involving the fourth state vanish ($\theta_{14} = \theta_{24} = \theta_{34} = 0$) one recovers the 3-flavor matrix in its standard parameterization. ii) For small values of the mixing angles involving the fourth mass eigenstate, it is $|U_{e4}|^2 = s_{14}^2$, $|U_{\mu4}|^2 \simeq s_{24}^2$ and $|U_{\tau4}|^2 \simeq s_{34}^2$, with an immediate physical interpretation of the new mixing angles. iii) With the leftmost positioning of the matrix $\tilde{R}_{34}$, in vacuum, the LBL $\nu_\mu \to \nu_e$ transition probability is independent of θ_{34} and of the associated *CP* phase δ_{34}.

III. FLAVOR CONVERSION AT SHORT BASELINES

Short-baseline experiments are sensitive only to the oscillations generated by the new squared-mass difference $\Delta m_{\mathrm{SBL}}^2 \sim 1$ eV^2, which in the 3 + 1 framework is $\Delta m_{\mathrm{SBL}}^2 = \Delta m_{41}^2 \simeq \Delta m_{42}^2 \simeq \Delta m_{43}^2$, taking into account that the solar squared-mass difference $\Delta m_{\mathrm{SOL}}^2 = \Delta m_{21}^2 \approx 7.4 \times 10^{-5}$ eV^2 and the atmospheric squared-mass difference $\Delta m_{\mathrm{ATM}}^2 = |\Delta m_{31}^2| \simeq |\Delta m_{32}^2| \approx 2.5 \times 10^{-3}$ eV^2 are much smaller (we use the notation $\Delta m_{jk}^2 = m_j^2 - m_k^2$).

The effective oscillation probabilities of the flavor neutrinos in short-baseline experiments are given by [15]

$$P_{\alpha\beta}^{(\mathrm{SBL})} \simeq \left| \delta_{\alpha\beta} - \sin^2 2\theta_{\alpha\beta}\sin^2\left(\frac{\Delta m_{41}^2 L}{4E}\right) \right|, \qquad (4)$$

where $\alpha, \beta = e, \mu, \tau, s$, L is the source-detector distance and E is the neutrino energy. The short-baseline oscillation

amplitudes depend only on the absolute values of the elements in the fourth column of the mixing matrix:

$$\sin^2 2\theta_{\alpha\beta} = 4|U_{\alpha 4}|^2|\delta_{\alpha\beta} - |U_{\beta 4}|^2|. \quad (5)$$

Hence, the transition probabilities of neutrinos and antineutrinos are equal and it is not possible to measure any CPV effect generated by the complex phases in the mixing matrix in short-baseline experiments.

The short-baseline anomalies in favor of the existence of active-sterile neutrino oscillations are:

(i) The LSND observation of an excess of $\bar{\nu}_e$-induced events in a $\bar{\nu}_\mu$ beam [16,17].

(ii) The Gallium neutrino anomaly [18–22], consisting in the disappearance of ν_e measured in the Gallium radioactive source experiments GALLEX [23] and SAGE [24].

(iii) The reactor antineutrino anomaly [25], which is a deficit of the rate of $\bar{\nu}_e$ observed in several reactor neutrino experiments in comparison with that expected from the calculation of the reactor neutrino fluxes [26,27].

IV. FLAVOR CONVERSION AT LONG BASELINES

Let us now come to the transition probability relevant for the LBL experiments T2K and NOνA. In Ref. [1], it has been shown that the probability can be written as the sum of three terms

$$P_{\mu e}^{4\nu} \simeq P^{\text{ATM}} + P_{\text{I}}^{\text{INT}} + P_{\text{II}}^{\text{INT}}. \quad (6)$$

The first term represents the positive definite atmospheric transition probability, which can be expressed as

$$P^{\text{ATM}} \simeq 4s_{23}^2 s_{13}^2 \sin^2 \Delta, \quad (7)$$

where $\Delta \equiv \Delta m_{31}^2 L/4E$ is the atmospheric oscillating frequency. The second term is related to the interference between the oscillations driven by the solar and atmospheric squared-mass splittings. This term, apart from higher order corrections, coincides with the standard interference term, which makes the transition probability sensitive to the CP phase $\delta \equiv \delta_{13}$. It can be written as

$$P_{\text{I}}^{\text{INT}} \simeq 8s_{13}s_{12}c_{12}s_{23}c_{23}(\alpha\Delta)\sin\Delta\cos(\Delta + \delta_{13}). \quad (8)$$

The third term is due to 4-flavor effects and is driven by the interference between the atmospheric frequency and the new large frequency introduced by the fourth mass eigenstate. It takes the form

$$P_{\text{II}}^{\text{INT}} \simeq 4s_{14}s_{24}s_{13}s_{23}\sin\Delta\sin(\Delta + \delta_{13} - \delta_{14}). \quad (9)$$

This term does not depend on Δm_{41}^2 because the fast oscillations are averaged by the finite resolution of the

detector. The transition probability depends on the three small mixing angles $s_{13}, s_{14}, s_{24} \simeq 0.15$, which can be all assumed to be of the same order ϵ. Another small quantity is the ratio of the solar and atmospheric squared-mass splittings $\alpha \equiv \Delta m_{12}^2/\Delta m_{13}^2 \simeq \pm 0.03$, which is of order ϵ^2. Remarkably, for values of the mixing angles indicated by the current global 3-flavor analyses [3–6] (for θ_{13}) and the $3 + 1$ fits [9–12] (for θ_{14} and θ_{24}), the size of the new (atmospheric-sterile) interference term is basically identical to that of the standard (solar-atmospheric) interference term [2]. This implies that T2K and NOνA are sensitive to both CP phases δ_{13} and δ_{14}.

Finally, we mention that the matter effects slightly modify the transition probability, leaving unaltered its decomposition in the sum of three contributions. We refer the reader to [1] for a detailed treatment of matter effects in the $3 + 1$ scheme. Here, we just recall that they introduce a dependency on the dimensionless quantity

$$v = \frac{2VE}{\Delta m_{31}^2}, \quad (10)$$

where

$$V = \sqrt{2}G_F N_e \quad (11)$$

is the constant matter potential along the neutrino trajectory in the Earth crust. We have $v \simeq 0.05$ in T2K and $v \simeq 0.17$ in NOνA at the energy corresponding to the first oscillation maximum ($E \simeq 0.6$ GeV in T2K, $E \simeq 2$ GeV in NOνA). Therefore, the matter effects are appreciable only in NOνA and confer to this experiment an enhanced sensitivity to the neutrino mass hierarchy.

V. DATA USED AND DETAILS OF THE ANALYSIS

For the determination of the two active-sterile mixing angles θ_{14} and θ_{24} we use the update of the analysis in Ref. [28] presented in Ref. [29]. We considered the data of the following three groups of experiments:

(A) The $\overset{(-)}{\nu}_\mu \to \overset{(-)}{\nu}_e$ appearance data of the LSND [17], MiniBooNE [30,31], BNL-E776 [32], KARMEN [33], NOMAD [34], ICARUS [35] and OPERA [36] experiments. The last two have been treated following the approach described in [37]. We did not consider the anomalous low-energy bins of the MiniBooNE experiment [30,31], according to the "pragmatic" approach advocated in Ref. [9].

(B) The following $\overset{(-)}{\nu}_e$ disappearance data (1) the data of the Bugey-4 [38], ROVNO91 [39], Bugey-3 [40], Gosgen [41], ILL [42], Krasnoyarsk [43], Rovno88 [44], SRP [45], Chooz [46], Palo Verde [47], Double Chooz [48], and Daya Bay [49] reactor antineutrino experiments with the new theoretical fluxes [25–27,50], (2) the data of the GALLEX [23] and SAGE [24] Gallium radioactive source experiments

with the statistical method discussed in Ref. [21], considering the recent ^{17}Ga(^{3}He, ^{3}H)^{17}Ge cross section measurement in Ref. [51], (3) the solar neutrino constraint on $\sin^2 2\theta_{ee}$ [22,52–55], and (4) the KARMEN [56] and LSND [57] $\nu_e + {}^{12}\text{C} \rightarrow {}^{12}\text{N}_{\text{g.s.}} + e^-$ scattering data [58], with the method discussed in Ref. [59].

(C) The constraints on the $\overset{(-)}{\nu}_\mu$ disappearance obtained from the data of the CDHSW experiment [60], from the analysis [61] of the data of atmospheric neutrino oscillation experiments, from the analysis [62,63] of the MINOS neutral-current data [64] and from the analysis of the SciBooNE-MiniBooNE data neutrino [65] and antineutrino [66] data. We have not included the IceCube results recently reported in [67]. However, this has no impact on our results because, as already noted in [29], these data modify the upper bounds on θ_{24} only for values of Δm_{41}^2 which are lower than ~ 1 eV^2. This conclusion is corroborated by the numerical analysis performed in [12].

Concerning the LBL experiments, we use the preliminary data released at the Neutrino 2016 and ICHEP 2016 conferences by the NOνA [7] and T2K [8] collaborations, considering the neutrino and antineutrino data sets, and including both the appearance and disappearance channels. In order to calculate the theoretical expectation for the total number of events and their binned spectra in the reconstructed neutrino energy, we use the software GLoBES [68,69]. As input information we use the unoscillated ν_μ and $\bar{\nu}_\mu$ fluxes extrapolated at the far detector from Ref. [70,71] for T2K and from Ref. [72] for NOνA. The analysis for the appearance channel is performed using the total rate information as in [1,2], which presents very small differences with respect to the analysis done using the full energy spectrum. This is due to three factors: (i) the off-axis configuration of NOνA and T2K, which leads to a narrow energy spectrum peaked around the first oscillation maximum, (ii) the limited statistics currently available in the appearance channel both in NOνA and T2K, and (iii) the smearing induced by the finite energy resolution of the far detectors. Differently, for the disappearance channel we perform a full spectral analysis of the far detector event distribution, since in this case the energy information has a crucial role.

In the standard 3-flavor case, the free parameters in the analysis are the atmospheric mass splitting Δm_{32}^2, the two mixing angles θ_{13}, θ_{23} and the CP phase δ_{13}. In the 4-flavor analysis, in addition, we consider as free parameters Δm_{41}^2, θ_{14}, θ_{24} and the CP phase δ_{14}. We fix $\theta_{34} = 0$, because the perturbations induced by nonzero θ_{34} are very small in T2K and NOνA. We have explicitly checked numerically that for nonzero values of θ_{34} currently allowed by data, the oscillation probabilities in both the appearance and disappearance channels are almost indistinguishable from

those calculated with $\theta_{34} = 0$. Finally, we mention that both in the 3-flavor and 4-flavor analyses we fix the solar mass-mixing parameters at their best-fit values obtained in the global 3-flavor analysis [3].

As pointed out in Ref. [1], in the 4-flavor scenario, the analysis has to deal with the fact that the near detectors in the long-baseline experiments T2K and NOνA are sensitive to the oscillations induced by the extra sterile neutrino. The neutrino fluxes used in the standard analysis are constrained with the information extracted from the near detectors under the assumption of no oscillation at short baselines, which is true only for three flavors. With the addition of an extra neutrino with $\Delta m_{41}^2 \sim O(1 \text{ eV}^2)$, the survival probability for ν_μ at the near detector can be approximated as

$$P_{\mu\mu}^{4\nu,\text{ND}} \simeq 1 - 4\sin^2\theta_{24}\sin^2\left(\frac{\Delta m_{41}^2 L}{4E}\right). \quad (12)$$

Therefore, a suppression of the fluxes that depends on the parameters Δm_{41}^2, θ_{24} and on the energy is expected. A precision analysis of the LBL data in the $3 + 1$ scheme would require the simultaneous treatment of the near and far detector. However, the spectrum of events expected at the near detector is problematic to reproduce, since many details are not accessible from outside the collaborations. To circumvent this problem we have incorporated the effects of the oscillation at the near detector using the following approximate procedure. We have corrected the expected distribution of events at the far detector multiplying it by the energy dependent factor $1/P_{\mu\mu}^{4\nu,\text{ND}}$, taking its averaged value in each energy bin. In this way, we approximately untie the far detector fluxes from their dependency on the oscillations occurred at the near detector. We have checked that these corrections introduce small modifications on our final results. Hence, our approximate approach is justified. However, we stress that a more detailed analysis in the $3 + 1$ scheme should incorporate the simultaneous fit of the native neutrino fluxes with the near and far detector data for varying values of the parameters Δm_{41}^2 and θ_{24}. At the moment, this is possible only from inside the experimental collaborations.

As a separate analysis, we constrain the value of θ_{13} using the far-to-near ratios of the reactor θ_{13}-sensitive experiments Daya-Bay and RENO. Their data are analyzed using the total rate information following the approach described in Ref. [73]. For both experiments, we have used the latest data [74,75] based, respectively, on 1230 live days (Daya Bay) and 500 live days (RENO), recently released at the Neutrino 2016 conference. Since the fast oscillations induced by Δm_{14}^2 are averaged out at both near and far detector sites, the far-to-near ratios of Daya Bay and RENO are not sensitive to 4-flavor effects. Therefore, the estimate of θ_{13} is identical in the 3-flavor and $3 + 1$ schemes.

VI. NUMERICAL RESULTS

A. Constraints on the new mixing angles (θ_{14}, θ_{24}) and the new *CP* phase δ_{14}

Figure 1 and 2 represent the bidimensional projections of the $\Delta\chi^2$ for normal hierarchy (NH) and inverted hierarchy (IH) in the planes [$\sin^2\theta_{14}, \delta_{14}$], [$\sin^2\theta_{14}, \sin^2\theta_{24}$] and [$\delta_{14}, \sin^2\theta_{24}$] for the top left, bottom left and bottom right panels respectively. The three contours are drawn for $\Delta\chi^2 = 2.3, 4.6, 6.0$, corresponding to 68%, 90% and 95% for 2 d.o.f. The allowed regions in the [$\sin^2\theta_{14}, \sin^2\theta_{24}$] plane are almost the same of those (not shown) that we obtain from the fit of the SBL data taken alone. This finding can be understood by observing that the SBL experiments currently dominate over the LBL ones in the determination of the two new mixing angles. We find that the overall goodness of fit is satisfactory (GoF = 24%), while the parameter goodness of fit (see [76] for its definition), which measures the statistical compatibility between the (discordant) appearance and disappearance data sets, is lower (GoF = 7%). This implies that even if the closed contours presented for the two new mixing angles θ_{14} and θ_{24} exclude zero with high significance (more than six standard deviations), one cannot naively interpret this circumstance
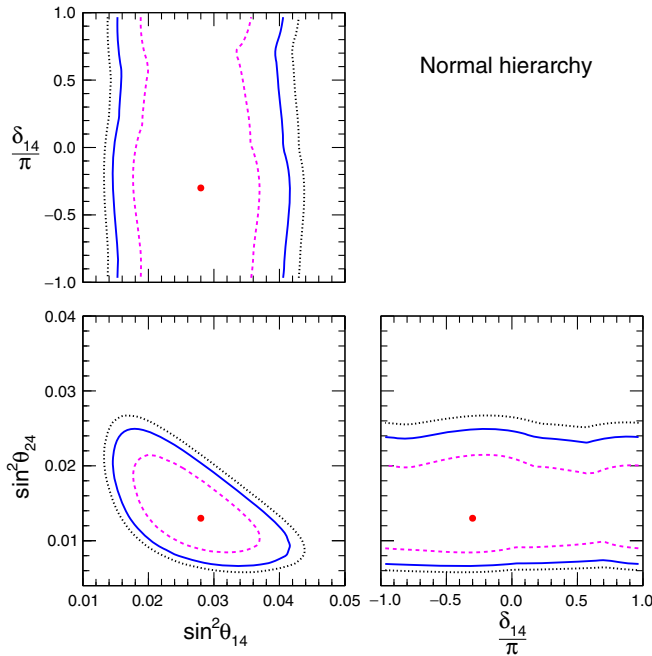

FIG. 1. Regions allowed by the combination of the SBL and LBL data (T2K and NOνA) together with the θ_{13}-sensitive reactor results for the NH case. The left-bottom panel reports the projection on the plane of the two mixing angles (θ_{14}, θ_{24}). The other two panels display the constraints in the plane formed by each one of these two mixing angles and the new *CP* phase δ_{14}. The confidence levels correspond to 68%, 90% and 95% for 2 d.o.f ($\Delta\chi^2 = 2.3, 4.6, 6.0$), and the best-fit points are marked with a red point.
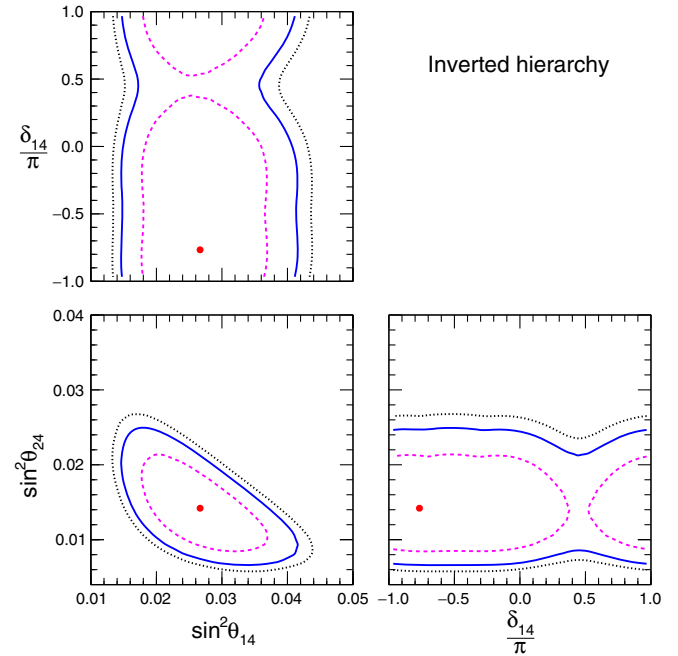

FIG. 2. Regions allowed by the combination of the SBL and LBL data (T2K and NOνA) together with the θ_{13}-sensitive reactor results for the IH case. The left-bottom panel reports the projection on the plane of the two mixing angles (θ_{14}, θ_{24}). The other two panels display the constraints in the plane formed by each one of these two mixing angles and the new *CP* phase δ_{14}. The confidence levels correspond to 68%, 90% and 95% for 2 d.o.f ($\Delta\chi^2 = 2.3, 4.6, 6.0$), and the best-fit points are marked with a red point.

as an evidence for sterile neutrinos. In addition, we mention that light sterile neutrinos, unless dressed with new properties, are in strong tension with cosmological data (see, for example, [77–81]).

The preferred values of $\sin^2\theta_{14}$ and $\sin^2\theta_{24}$ lie in the range [0.01-0.03], which means that the new mixing angles θ_{14} and θ_{24} are of the same order of magnitude of the standard mixing angle θ_{13} (we recall that $\sin^2\theta_{13} \simeq 0.025$). A quick estimate of the amplitude of the new interference term in Eq. (9) reveals that its size is similar to that of the standard interference term in Eq. (8). Therefore, it is quite natural to expect that the LBL data will posses some sensitivity to the new *CP* phase δ_{14}. This qualitative conclusion is validated by our numerical results displayed in the top left and bottom right panels of Figs. 1 and 2. It is important to observe that the input from the SBL experiments is essential for the extraction of the information on δ_{14} from the LBL setups, since these last ones have a very scarce sensitivity to θ_{14} and θ_{24}, and therefore are unable to constrain the amplitude of the new interference term in Eq. (9). In addition, we underline that also the precise determination of θ_{13} attained independently by the reactor experiments Daya Bay and RENO, plays a relevant role in constraining the new *CP* phase δ_{14}, because it helps to constrain the magnitude of the leading term in Eq. (7)

(proportional to s_{13}^2) and the amplitude of the two standard interference terms (which are both proportional to s_{13}). A comparison of our results with those presented in [1,2] shows that the 68% and 90% bounds on δ_{14} are slightly weaker, despite the improved statistics accumulated in the LBL data. This is due to having taken into account the uncertainty on θ_{14} and θ_{24}, which in [1,2] were both fixed to $\sin^2\theta_{14} = \sin^2\theta_{24} = 0.025$.

B. Correlation between the two *CP* phases δ_{13} and δ_{14}

Figure 3 shows the constraints in the plane of the two *CP* phases [δ_{14}, δ_{13}] for NH (IH) left panel (right panel). Also in this figure, the regions are obtained combining the SBL data, the LBL results from NOνA and T2K, and the data from Daya-Bay and RENO. In both mass hierarchies, the *CP*-conserving cases $\delta_{13} = 0, \pi$ are disfavored at $\Delta\chi^2 \simeq 2.7$. The best-fit value $\delta_{13} \simeq -\pi/2$, is basically the same obtained in the 3-flavor case (see the analyses [3–6]). This preference comes from the observation of an excess (deficit) of ν_e ($\bar{\nu}_e$) events with respect to the expectations for the appearance channel $\nu_\mu \to \nu_e$ ($\bar{\nu}_\mu \to \bar{\nu}_e$), when assuming a value of θ_{13} equal to the best-fit point of reactor experiments. In fact, Eq. (8) shows that, around the first oscillation maximum ($\Delta = \pi/2$), the standard interference term is proportional to $\sin\delta_{13}$.[2] This implies that this term is maximized (minimized) for neutrinos (antineutrinos) for $\delta_{13} = -\pi/2$ in agreement with the observed pattern. Our numerical analysis in the $3 + 1$ scheme reveals that the presence of the new interference terms does not spoil this picture. This behavior can be explained by observing that at the first oscillation maximum ($\Delta = \pi/2$) the new interference term is proportional to $\cos(\delta_{13} - \delta_{14})$, and therefore (in contrast to the standard term) its sign is the same for neutrinos and antineutrinos. We observe that for $\delta_{13} \simeq \delta_{14} \simeq -\pi/2$, the new interference term assumes its maximal positive value (for both neutrinos and antineutrinos). In the fit, the neutrino data set dominates over the (lower statistics) antineutrino data set and, as a consequence, the excess of ν_e's wins over the deficit of $\bar{\nu}_e$'s, driving the new *CP* phase to a best-fit value close to $\delta_{14} \simeq -\pi/2$. Finally, we note that the constraints on the new *CP* phase δ_{14} are very weak. This is imputable to the smaller amplitude of the new interference term when compared to the standard interference term.

C. Impact of sterile neutrinos on the standard neutrino properties

In the previous subsections, we have focused our discussion on the new parameters of the $3 + 1$ scheme and to the correlation among the two *CP* phases. However, it is of interest to see what happens to the estimates of the

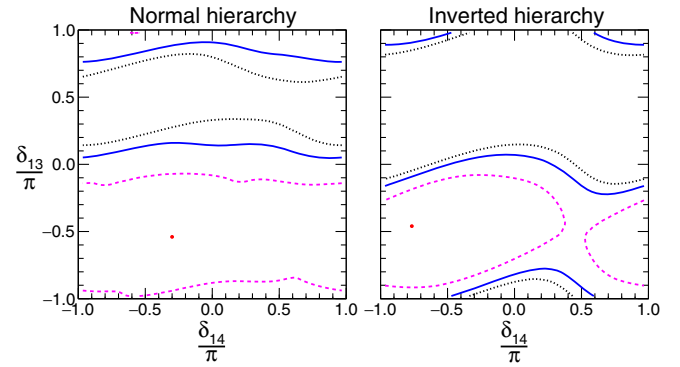FIG. 3. Regions allowed by the combination of the SBL and LBL data (T2K and NOνA) together with the θ_{13}-sensitive reactor results for NH (left panel) and IH (right panel) in the plane spanned by the two *CP* phases δ_{13} and δ_{14}. The confidence levels are the same ones used in Fig. 1.

standard parameters, which were marginalized in the figures shown until now. In particular, it seems of particular interest to assess the robustness or fragility of the estimate of the *CP* phase $\delta \equiv \delta_{13}$, the mass hierarchy and the mixing angle θ_{23}, which all are at the center of current investigations.

Figure 4 displays the regions allowed in the plane [$\sin^2 2\theta_{13}, \delta_{13}$] by the joint analysis of all the SBL experiments and the two LBL experiments T2K and NOνA. The two upper panels correspond to the 3-flavor framework,[3] while the two lower ones are obtained in the 4-flavor scheme. The two left (right) panels refer to NH (IH). The interval of θ_{13} identified by the reactor experiments at 68% C.L. (represented by the green vertical band) is displayed for the sake of comparison. In all cases, Δm_{32}^2 and the mixing angle θ_{23} are marginalized away. In addition, in the 4-flavor case, we marginalize over the two mixing angles (θ_{14}, θ_{24}) and the *CP* phase δ_{14}. The contours represented in the plots correspond to the same confidence levels reported in the previous plots. The comparison of the 3-flavor and 4-flavor allowed regions shows the following features: (i) the range allowed by LBL alone for θ_{13} is appreciably larger in the 4-flavor case. This is a consequence of the presence of the new interference term, which allows larger excursions of the transition

---

[2]We recall that the when passing from neutrino to antineutrino probability one has to invert the sign of all the *CP* phases.

[3]It should be noted that at the SBL experiments the 3-flavor effects are completely negligible. Consequently, one can adopt two different approaches when considering the 3-flavor scheme: (i) include the SBL data in the fit and (ii) exclude them from the fit. What changes between the two approaches is only the value of the absolute minimum of the χ^2. Following the first option, one obtains a much higher value than following the second one. This just corresponds to the fact that in the $3 + 1$ scheme the goodness of fit increases, because the sterile oscillations are able to fit the SBL data. However, when one is interested in parameter estimation, only the expansion of the χ^2 around its absolute minimum matters and the choice of including or not including the SBL data in the fit is irrelevant.
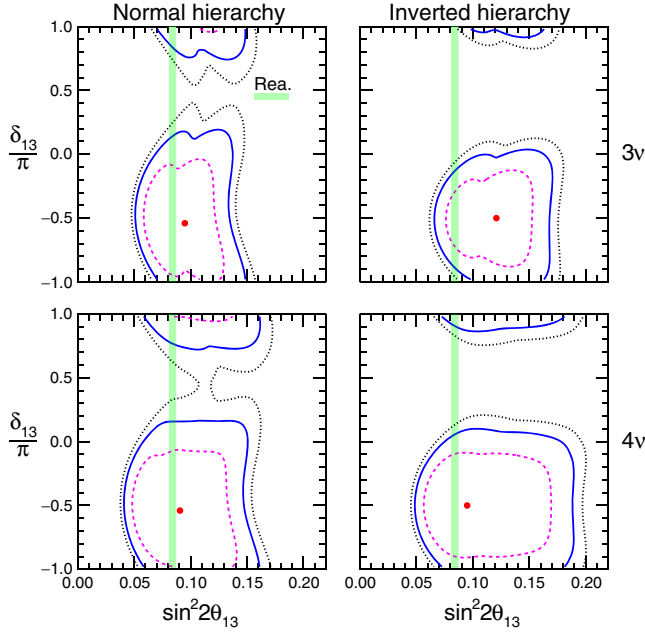
FIG. 4. Regions allowed in the plane $[\sin^2 2\theta_{13}, \delta_{13}]$ by the joint analysis of all the SBL experiments and the LBL experiments (T2K and NOνA). The interval of θ_{13} identified by the reactor experiments (green vertical band) is displayed for the sake of comparison. The left (right) panels represent the NH (IH) case. The upper (lower) panels refer to the 3-flavor (4-flavor) scheme. The confidence levels are the same reported in Fig. 1.

FIG. 5. Regions allowed in the plane $[\sin^2 \theta_{23}, \Delta m^2_{32}]$ by the joint analysis of all the SBL, the LBL data (T2K and NOνA), together with the θ_{13}-sensitive reactor results. The left (right) panels represent the NH (IH) case. The upper (lower) panels refer to the 3-flavor (4-flavor) scheme. The confidence levels are the same reported in Fig. 1.

probability from its average value. However, one can understand that, once the reactor data sensitive to θ_{13} (Daya Bay and RENO) are included in the fit, θ_{13} is "fixed" with high precision in both 3-flavor and 4-flavor schemes, (ii) the constraints on the CP phase δ_{13} are basically identical in the two schemes. In both cases, there is a preference (rejection) of values of $\sin \delta_{13} < 0$ ($\sin \delta_{13} > 0$). We have already discussed this point in the description of Fig. 3 concerning the correlation on the two CP phases, and (iii) in both schemes the allowed regions, at low confidence levels, present two lobes, which are more pronounced in the 3-flavor case. This feature is imputable to the swap of the best-fit value of θ_{23} among the two quasi-degenerate nonmaximal solutions, one in the lower octant (LO) and the other one in the higher octant (HO). We will discuss further this point when commenting Fig. 5.

Figure 4 also evidences appreciable differences between the two cases of NH and IH, which can be traced to the presence of the matter effects. As discussed in Sec. IV, the matter potential tends to increase (decrease) the theoretically expected ν_e rate in the case of NH (IH). The opposite is true for $\bar{\nu}_e$'s but their weight in the analysis is lower, so the neutrino data sets dominate. In addition, as discussed in Sec. IV, the NOνA ν_e data are more sensitive than the T2K ν_e data to the matter effects. More specifically, the following differences among the two hierarchies emerge, which are present both in the 3-flavor and 4-flavor
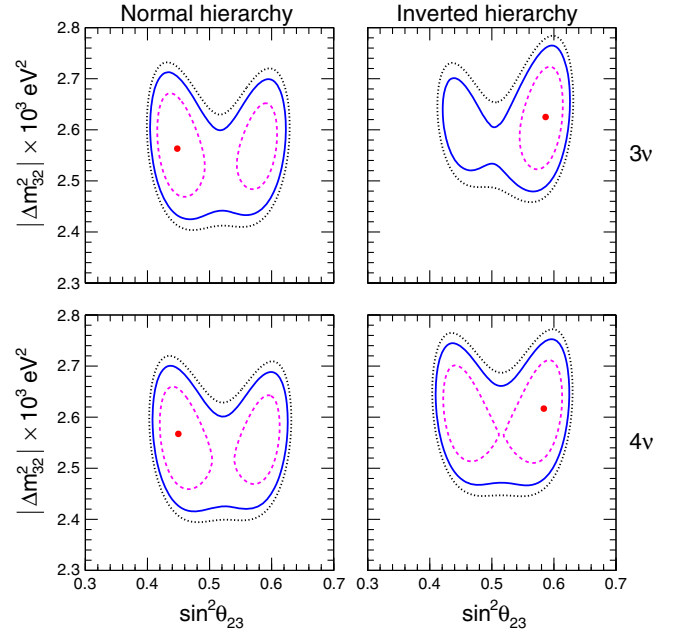
schemes. The regions obtained for the case of IH are shifted towards larger values of θ_{13} and are slightly wider in the variable θ_{13} with respect to those obtained in the NH case. In addition, in the IH case, the fit tends to prefer (reject) values of $\sin \delta_{13} < 0$ ($\sin \delta_{13} > 0$) in a more pronounced way.

After marginalizing over all parameters we can calculate the $\Delta\chi^2(\text{IH} - \text{NH})$ difference between normal and inverted hierarchy

$$\Delta\chi^2(\text{IH} - \text{NH}) = \chi^2_{\min}(\text{IH}) - \chi^2_{\min}(\text{NH}). \quad (13)$$

For the 3-flavors (4-flavors) analysis of the LBL data alone, we obtain $\Delta\chi^2(\text{IH} - \text{NH}) \simeq 1.0$ (0.8). Therefore, these data are (still) not sensitive to the mass hierarchy. The situation sensibly changes when the reactor experiments sensitive to θ_{13} are included in the fit. In fact, the combination of LBL and reactor provides a slight preference for NH: $\Delta\chi^2(\text{IH} - \text{NH}) \simeq 2.0$ (1.3) in the 3-flavor (4-flavors) case. The reduced value obtained in the $3 + 1$ framework is due to the inevitable widening of the parameter space in the presence of an additional neutrino. The preference for the NH case can be understood comparing the allowed regions from T2K and NOνA with the constraint on $\sin^2 2\theta_{13}$ from reactor experiments (vertical green band in Fig. 4). One notes that there is a better agreement for NH, whereas for IH the separation between the two best-fit points is at the level of about $\sim 1\sigma$.

Let us now come to the estimate of the standard mixing angle θ_{23}. Recently, the disappearance analysis of the NOνA collaboration [7] has reported a preference for nonmaximal θ_{23} at the level of 2.5σ. The latest 3-flavor global fits [4,5] have shown that this feature persists at the level of about 2σ even when other datasets are included in the analysis. Given the important role of the atmospheric angle θ_{23} in the context of model building, it seems opportune to assess the estimate of such a parameter in the enlarged $3+1$ scheme.

We recall that, in the 3-flavor framework, the disappearance channel is sensitive to possible deviations from maximal mixing but it is blind to the octant of θ_{23}. This occurs because the $\nu_\mu \rightarrow \nu_\mu$ disappearance probability is proportional to $\sin^2 2\theta_{23}$. Therefore, if only the disappearance channel data are included in the analysis, the allowed ranges are symmetrical with respect to $\sin^2\theta_{23} = 0.5$. This symmetry is broken when one considers also the appearance channel. This happens because the $\nu_\mu \rightarrow \nu_e$ transition probability is octant sensitive since its leading term depends on $\sin^2\theta_{23}$. In the 4-flavor scheme, the disappearance probability remains basically unaltered, so one expects that the sensitivity to potential deviations from maximal mixing remains unaltered. In contrast, the appearance probability is profoundly affected by the new interference term, which, as recently shown in [82], leads to a loss of sensitivity to the octant of θ_{23}.

Figure 5 reports the allowed regions in the plane $[\sin^2\theta_{23}, \Delta m_{32}^2]$, all the other parameters having being marginalized away. The left (right) panels refer to normal (inverted) hierarchy, while the upper (lower) panels refer to the 3-flavor (4-flavor) case. In both schemes, we have included in the analysis all the SBL data, the LBL results from T2K and NOνA (both appearance and disappearance channels), and the θ_{13}-sensitive reactor experiments. The results reported in the upper panels show a weak preference for nonmaximal mixing in the 3-flavor scenario. We note that there is a change in the preferred octant when switching from normal to inverted hierarchy. This is a consequence of the anticorrelation between θ_{13} and θ_{23}, introduced by the appearance data set: the lower θ_{13} the higher the value of θ_{23}. In NH, we find a negligible preference for the lower octant ($\theta_{23} < 45^0$). In IH, the effect is more pronounced and the higher octant ($\theta_{23} > 45^0$) is favored at a non-negligible statistical level. The two lower panels depict how the situation changes in the 4-flavor scheme. We can observe that the allowed regions becomes basically symmetric around maximal mixing. As expected from the discussion above, in the 4-flavor scheme, the sensitivity to the θ_{23} octant gets lost.

In order to clarify this picture, we present in Fig. 6 the marginalized $\Delta\chi^2$ as a function of $\sin^2\theta_{23}$. The left (right) panel corresponds to NH (IH). The black solid line indicates the 3-flavor case, while the red dashed line refers to the $3+1$ scheme. In both NH and IH cases, in the
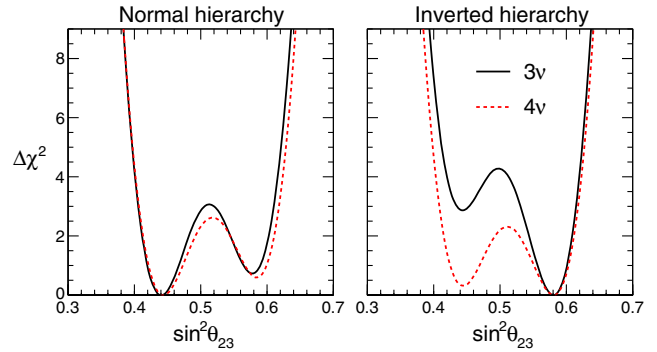

FIG. 6. Marginalized $\Delta\chi^2$ for the parameter $\sin^2\theta_{23}$ for NH (left panel) and IH (right panel). The black solid line indicates the 3-flavor case, while the red dashed line refers to the $3+1$ scheme.

4-flavor scheme, nonmaximal mixing is disfavored approximately at $\Delta\chi^2 \simeq 2.5$ (corresponding almost to 90% C.L. for 1 d.o.f.). Therefore, the weak preference for nonmaximal θ_{23} originating from (part of) the disappearance channel data is a stable feature, which is independent of the scheme adopted (3-flavor or 4-flavor). In contrast, we see that the preference for $\theta_{23} > 45^0$ found in IH completely disappears in the $3+1$ scheme. We finally note that this behavior is in line with the results of the sensitivity study performed in [82], where it has been shown that even in a future experiment like DUNE, which will make use of a high-intensity broad-band neutrino beam, the sensitivity to the octant drastically decreases in the $3+1$ scheme. Our analysis performed with the real data confirms such a general behavior, showing that the indication on the octant of θ_{23} becomes a fragile feature in the $3+1$ framework.

VII. CONCLUSIONS

We have shown that, within the $3+1$ scheme, the combination of the existing SBL data with the LBL results coming from the two currently running experiments NOνA and T2K, enables us to simultaneously constrain two active-sterile mixing angles θ_{14} and θ_{24} and two CP phases $\delta_{13} \equiv \delta$ and δ_{14}, although the constraints on this last CP phase are still weak. The two mixing angles are basically determined by the SBL data, while the two CP phases are identified by the LBL experiments, once the information coming from the SBL setups is taken into account. We have also assessed the robustness or fragility of the estimates of the standard 3-flavor properties in the more general $3+1$ scheme. To this regard we found that (i) the indication of CP-violation found in the 3-flavor analyses persists also in the $3+1$ scheme, with $\delta_{13} \equiv \delta$ having still its best-fit value around $-\pi/2$, (ii) the 3-flavor weak hint in favor of the normal hierarchy becomes even less significant when sterile neutrinos come into play, and (iii) the

weak indication of nonmaximal θ_{23} (driven by NOνA disappearance data) persists in the $3+1$ scheme, where maximal mixing is disfavored at almost the 90% C.L. in both normal and inverted mass hierarchy; iv) the preference in favor of one of the two octants of θ_{23} found in the 3-flavor framework (higher octant for inverted mass hierarchy) is completely washed out in the $3+1$ scheme. We hope that our joint analysis of SBL and LBL data in the $3+1$ scheme may serve as a guide for more comprehensive analyses and may increase the awareness of the neutrino community towards the important role of LBL experiments in the search of *CP* violation induced by light sterile neutrinos.

[1] N. Klop and A. Palazzo, Phys. Rev. D **91,** 073017 (2015).

[2] A. Palazzo, Phys. Lett. B **757,** 142 (2016).

[3] F. Capozzi, E. Lisi, A. Marrone, D. Montanino, and A. Palazzo, Nucl. Phys. **B908,** 218 (2016).

[4] A. Marrone, in *Proc. of 27th International Conference on Neutrino Physics and Astrophysics*, July 4–9, 2016, London.

[5] I. Esteban, M. C. Gonzalez-Garcia, M. Maltoni, I. Martinez-Soler, and T. Schwetz, J. High Energy Phys. 01 (2017) 087.

[6] D. V. Forero, M. Tortola, and J. W. F. Valle, Phys. Rev. D **90,** 093006 (2014).

[7] P. Vahle, in *Proc. of 27th International Conference on Neutrino Physics and Astrophysics*, July 4–9, 2016, London.

[8] K. Iwamoto, in *Proc. of 38th International Conference on High Energy Physics*, August 2016, Chicago.

[9] C. Giunti, M. Laveder, Y. Li, and H. Long, Phys. Rev. D **88,** 073008 (2013).

[10] J. Kopp, P. A. N. Machado, M. Maltoni, and T. Schwetz, J. High Energy Phys. 05 (2013) 050.

[11] G. H. Collin, C. A. Arguelles, J. M. Conrad, and M. H. Shaevitz, Nucl. Phys. **B908,** 354 (2016).

[12] G. H. Collin, C. A. Argelles, J. M. Conrad, and M. H. Shaevitz, Phys. Rev. Lett. **117,** 221801 (2016).

[13] S. K. Agarwalla, S. S. Chatterjee, A. Dasgupta, and A. Palazzo, J. High Energy Phys. 02 (2016) 111.

[14] S. K. Agarwalla, S. S. Chatterjee, and A. Palazzo, J. High Energy Phys. 09 (2016) 016.

[15] S. M. Bilenky, C. Giunti, and W. Grimus, Eur. Phys. J. C **1,** 247 (1998).

[16] C. Athanassopoulos *et al.* (LSND Collaboration), Phys. Rev. Lett. **75,** 2650 (1995).

[17] A. Aguilar *et al.* (LSND Collaboration), Phys. Rev. D **64,** 112007 (2001).

[18] J. N. Abdurashitov *et al.* (SAGE Collaboration), Phys. Rev. C **73,** 045805 (2006).

[19] M. Laveder, Nucl. Phys. B, Proc. Suppl. **168,** 344 (2007).

[20] C. Giunti and M. Laveder, Mod. Phys. Lett. A **22,** 2499 (2007).

[21] C. Giunti and M. Laveder, Phys. Rev. C **83,** 065504 (2011).

[22] C. Giunti, M. Laveder, Y. Li, Q. Liu, and H. Long, Phys. Rev. D **86,** 113014 (2012).

[23] F. Kaether, W. Hampel, G. Heusser, J. Kiko, and T. Kirsten, Phys. Lett. B **685,** 47 (2010).

[24] J. N. Abdurashitov *et al.* (SAGE Collaboration), Phys. Rev. C **80,** 015807 (2009).

[25] G. Mention, M. Fechner, T. Lasserre, T. A. Mueller, D. Lhuillier, M. Cribier, and A. Letourneau, Phys. Rev. D **83,** 073006 (2011).

[26] T. A. Mueller, D. Lhuillier, M. Fallot, A. Letourneau, S. Cormon, M. Fechner, L. Giot, T. Lasserre, J. Martino, G. Mention, A. Porta, and F. Yermia, Phys. Rev. C **83,** 054615 (2011).

[27] P. Huber, Phys. Rev. C **84,** 024617 (2011).

[28] S. Gariazzo, C. Giunti, M. Laveder, Y. Li, and E. Zavanin, J. Phys. G **43,** 033001 (2016).

[29] C. Giunti, in *Proc. of 27th International Conference on Neutrino Physics and Astrophysics (Neutrino 2016)*, London, United Kingdom, July 4–9, 2016.

[30] A. A. Aguilar-Arevalo *et al.* (MiniBooNE Collaboration), Phys. Rev. Lett. **102,** 101802 (2009).

[31] A. Aguilar-Arevalo *et al.* (MiniBooNE Collaboration), Phys. Rev. Lett. **110,** 161801 (2013).

[32] L. Borodovsky *et al.* (BNL-E776 Collaboration), Phys. Rev. Lett. **68,** 274 (1992).

[33] B. Armbruster *et al.* (KARMEN Collaboration), Phys. Rev. D **65,** 112001 (2002).

[34] P. Astier *et al.* (NOMAD Collaboration), Phys. Lett. B **570,** 19 (2003).

[35] M. Antonello *et al.* (ICARUS Collaboration), Eur. Phys. J. C **73,** 2599 (2013).

[36] N. Agafonova *et al.* (OPERA Collaboration), J. High Energy Phys. 07 (2013) 004.

[37] A. Palazzo, Phys. Rev. D **91,** 091301 (2015).

[38] Y. Declais, H. de Kerret, B. Lefièvre, M. Obolensky, A. Etenko, Y. Kozlov, I. Machulin, V. Martemianov, L. Mikaelyan, M. Skorokhvatov, S. Sukhotin, and

V. Vyrodov (Bugey Collaboration), Phys. Lett. B **338**, 383 (1994).

[39] A. Kuvshinnikov, L. Mikaelyan, S. Nikolaev, M. Skorokhvatov, and A. Etenko, JETP Lett. **54**, 253 (1991).

[40] B. Achkar *et al.* (Bugey Collaboration), Nucl. Phys. **B434**, 503 (1995).

[41] G. Zacek, F. v. Feilitzsch, R. L. Mössbauer, L. Oberauer, V. Zacek, F. Boehm, P. H. Fisher, J. L. Gimlett, A. A. Hahn, H. E. Henrikson, H. Kwon, J. L. Vuilleumier, and K. Gabathuler (CalTech-SIN-TUM Collaboration), Phys. Rev. D **34**, 2621 (1986).

[42] A. Hoummada, S. Lazrak Mikou, G. Bagieu, J. Cavaignac, and D. Holm Koang, Appl. Radiat. Isot. **46**, 449 (1995).

[43] G. S. Vidyakin *et al.* (Krasnoyarsk Collaboration), Sov. Phys. JETP **71**, 424 (1990).

[44] A. I. Afonin *et al.*, Sov. Phys. JETP **67**, 213 (1988).

[45] Z. D. Greenwood, W. R. Kropp, M. A. Mandelkern, S. Nakamura, E. L. Pasierb-Love, L. R. Price, F. Reines, S. P. Riley, H. W. Sobel, N. Baumann, and H. S. Gurr, Phys. Rev. D **53**, 6054 (1996).

[46] M. Apollonio *et al.* (CHOOZ Collaboration), Eur. Phys. J. C **27**, 331 (2003).

[47] F. Boehm, J. Busenitz, B. Cook, G. Gratta, H. Henrikson, J. Kornis, D. Lawrence, K. B. Lee, K. McKinny, L. Miller, V. Novikov, A. Piepke, B. Ritchie, D. Tracy, P. Vogel, Y-F. Wang, and J. Wolf (Palo Verde Collaboration), Phys. Rev. D **64**, 112001 (2001).

[48] Y. Abe *et al.* (Double Chooz Collaboration), J. High Energy Phys. 10 (2014) 86.

[49] F. P. An *et al.* (Daya Bay Collaboration), Phys. Rev. Lett. **116**, 061801 (2016).

[50] K. N. Abazajian *et al.*, arXiv:1204.5379.

[51] D. Frekers, H. Ejiri, H. Akimune, T. Adachi, B. Bilgier *et al.*, Phys. Lett. B **706**, 134 (2011).

[52] C. Giunti and Y. Li, Phys. Rev. D **80**, 113007 (2009).

[53] A. Palazzo, Phys. Rev. D **83**, 113013 (2011).

[54] A. Palazzo, Phys. Rev. D **85**, 077301 (2012).

[55] A. Palazzo, Mod. Phys. Lett. A **28**, 1330004 (2013).

[56] B. Armbruster *et al.* (KARMEN Collaboration), Phys. Rev. C **57**, 3414 (1998).

[57] L. B. Auerbach *et al.* (LSND Collaboration), Phys. Rev. C **64**, 065501 (2001).

[58] J. Conrad and M. Shaevitz, Phys. Rev. D **85**, 013017 (2012).

[59] C. Giunti and M. Laveder, Phys. Lett. B **706**, 200 (2011).

[60] F. Dydak *et al.* (CDHSW Collaboration), Phys. Lett. B **134**, 281 (1984).

[61] M. Maltoni and T. Schwetz, Phys. Rev. D **76**, 093005 (2007).

[62] D. Hernandez and A. Y. Smirnov, Phys. Lett. B **706**, 360 (2012).

[63] C. Giunti and M. Laveder, Phys. Rev. D **84**, 093006 (2011).

[64] P. Adamson *et al.* (MINOS Collaboration), Phys. Rev. Lett. **107**, 011802 (2011).

[65] K. B. M. Mahn *et al.* (SciBooNE-MiniBooNE Collaboration), Phys. Rev. D **85**, 032007 (2012).

[66] G. Cheng *et al.* (SciBooNE-MiniBooNE Collaboration), Phys. Rev. D **86**, 052009 (2012).

[67] M. G. Aartsen *et al.* (IceCube Collaboration), Phys. Rev. Lett. **117**, 071801 (2016).

[68] P. Huber, M. Lindner, and W. Winter, Comput. Phys. Commun. **167**, 195 (2005).

[69] P. Huber, J. Kopp, M. Lindner, M. Rolinec, and W. Winter, Comput. Phys. Commun. **177**, 432 (2007).

[70] K. Abe *et al.* (T2K Collaboration), Phys. Rev. D **87**, 012001 (2013); **87**, 019902(A) (2013).

[71] M. Ravonel Salzgeber (T2K Collaboration), arXiv: 1508.06153.

[72] D. R. Rocco, Ph.D. thesis, University of Minnesota, 2016, http://lss.fnal.gov/archive/thesis/2000/fermilab-thesis-2016-15.pdf.

[73] A. Palazzo, J. High Energy Phys. 10 (2013) 172.

[74] Z. Yu, in *Proc. of 27th International Conference on Neutrino Physics and Astrophysics*, July 4–9, 2016, London.

[75] K. K. Joo, in *Proc. of 27th International Conference on Neutrino Physics and Astrophysics*, July 4–9, 2016, London.

[76] M. Maltoni and T. Schwetz, Phys. Rev. D **68**, 033020 (2003).

[77] S. Hannestad, I. Tamborra, and T. Tram, J. Cosmol. Astropart. Phys. 07 (2012) 025.

[78] B. Dasgupta and J. Kopp, Phys. Rev. Lett. **112**, 031803 (2014).

[79] S. Hannestad, R. S. Hansen, and T. Tram, Phys. Rev. Lett. **112**, 031802 (2014).

[80] N. Saviano, A. Mirizzi, O. Pisanti, P. D. Serpico, G. Mangano, and G. Miele, Phys. Rev. D **87**, 073006 (2013).

[81] M. Archidiacono, S. Gariazzo, C. Giunti, S. Hannestad, R. Hansen, M. Laveder, and T. Tram, J. Cosmol. Astropart. Phys. 08 (2016) 067.

[82] S. K. Agarwalla, S. S. Chatterjee, and A. Palazzo, Phys. Rev. Lett. **118**, 031804 (2017).